ACS APPLIED MATERIALS & INTERFACES

Research Article

www.acsami.org

"Butterfly Effect" in CuO/Graphene Composite Nanosheets: A Small Interfacial Adjustment Triggers Big Changes in Electronic Structure and Li-Ion Storage Performance

Xiaoting Zhang,[∥,†] Jisheng Zhou,[∥,†] Huaihe Song,*[,†] Xiaohong Chen,[†] Yu. V. Fedoseeva,[‡,§] A. V. Okotrub,[‡,§] and L. G. Bulusheva[‡,§]

[†]State Key Laboratory of Chemical Resource Engineering, Key Laboratory of Carbon Fiber and Functional Polymers, Ministry of Education, Beijing University of Chemical Technology, Beijing 100029, China

[‡]Nikolaev Institute of Inorganic Chemistry, Siberian Branch of Russian Academy of Sciences, 630090 Novosibirsk, Russia

[§]Novosibirsk State University, 630090 Novosibirsk, Russia

Supporting Information

ABSTRACT: Generally speaking, excellent electrochemical performance of metal oxide/graphene nanosheets (GNSs) composite is attributed to the interfacial interaction (or "synergistic effect") between constituents. However, there are no any direct observations on how the electronic structure is changed and how the properties of Li-ion storage are affected by adjusting the interfacial interaction, despite of limited investigations on the possible nature of binding between GNSs and metal oxide. In this paper, CuO nanosheets/GNSs composites with a little Cu_2O (ca. 4 wt %) were utilized as an interesting model to illustrate directly the changes of interfacial nature as well as its deep influence on the electronic structure and Li-ion storage performance of composite. The interfacial adjustment was successfully fulfilled by removal of Cu_2O in the composite by $NH_3{\cdot}H_2O$. Formation of Cu−O−C bonds on interfaces both between CuO and GNSs, and Cu_2O and GNSs in the original CuO/GNSs composites was detected. The small interfacial alteration by removal of the little Cu_2O results in the obvious changes in electronic structure, such as weakening of covalent Cu−O−C interfacial interaction and recovery of π bonds in graphene, and simultaneously leads to variations in electrochemical performance of composites, including a 21% increase of reversible capacity, degradation of cyclic stability and rate-performance, and obvious increase of charge-transfer resistance, which can be called a "butterfly effect" in graphene-based metal oxide composites. These interesting phenomena could be helpful to design not only the high-performance graphene/metal oxide anode materials but also various advanced graphene-based composites used in the other fields such as sensors, catalysis, fuel cells, solar cells, etc.

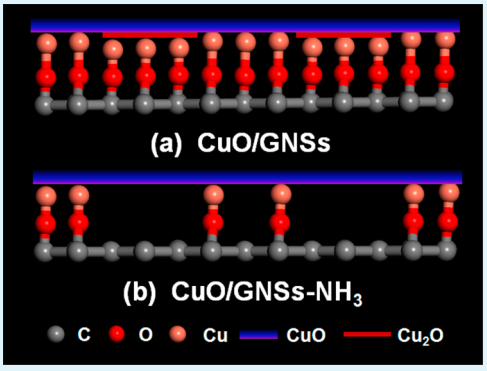

KEYWORDS: *interfacial interaction, graphene, CuO, Cu_2O, lithium-ion battery, NEXAFS*

1. INTRODUCTION

Transition metal oxides including Fe_2O_3, Co_3O_4, NiO, and CuO have attracted much attention because of their eco-friendliness, low cost, and high theoretical specific capacity.[1−5] However, some of their drawbacks, such as low conductivity, and pulverization and aggregation caused by large volume expansion, lead to their rapid capacity attenuation during charge/discharge process and hinder severely their practical application in future. To improve the electrochemical performance, one of basic strategies is to design various nanocarbon-based metal oxide anode materials.[6] Compared with other carbon materials such as carbon nanotube and amorphous carbon coating layer, graphene as an emerging two-dimensional nanocarbon possesses more excellent performance. Therefore, the rising discovery of graphene triggers a pervasive fever for design of graphene-based metal oxide anode materials.[7−9]

Except the charming properties of graphene itself, another novelty of graphene-based composite anode is interfacial interaction between metal oxide and graphene, which not only can control the morphology and size of inorganic particles grown on the surface of GNSs[6,10,11] but also can affect the charge transport and rate performance as well as ability of withstanding repeating lithiation/delithiation of electrode materials.[7,9,12] Up to now, many researchers have attributed improvement of electrochemical performance of graphene-based metal oxide anode materials to so-called "synergistic effect".[9,13−15] However, most of previous efforts were mainly focused on the preparation strategies and Li-ion storage

Received: August 3, 2014
Accepted: September 16, 2014
Published: September 16, 2014

measurement of graphene-based composites. To the best of our knowledge, there is a limited understanding of exact nature of interfacial interaction and electronic structure of composite as well as its influence on electrochemical performance of composites. In our previous work, we found a covalent Fe−O−C bonding between Fe_3O_4 and GNSs and proved that this interaction can enhance the high-rate performance as well as longlife cyclic ability of Fe_3O_4/GNSs anode.[7] Similarly, Zhou et al. also discovered that C−O−Ni interaction is helpful in improvement of Li-ion storage of NiO/graphene composites.[9] Besides enhancing the electrochemical performance of composite anode materials, this kind of strongly covalent couple exerted positive influence over many other applications of graphene-based metal oxide composites. For example, Liang et al. detected possible Co−O−C/Co−N−C bond interaction in Co_3O_4/N-doped graphene composite, which greatly improves the electrocatalytic activity of oxygen reduction reaction of composite.[12] Nevertheless, it can be seen from the few reports that the interfacial interaction will open up a new way for preparation of new-type graphene-based composites with high performance.

Moreover, to design a better graphene-based composite anode, it is not enough to just recognize the nature of bonding. Naturally, deep understanding of how the interfacial interaction in composite system affect the electronic structure of composites, especially of graphene, and what is the relationship between electronic structures and electrochemical performance of composites need to be done, which is helpful to illuminate the root causes of improvement of electrochemical performance of metal oxide by graphene. However, the case has not yet to be investigated in any graphene/metal oxide system due to the fact that it is difficult to find a suitable system to adjust its interface and exploring the subsequent influence on electronic structure and electrochemical performance.

In this paper, we designed a CuO nanosheets/graphene composite with a small quantity of Cu_2O, which owns a complex interface composed of covalent Cu−O−C bonds in both CuO/GNSs and Cu_2O/GNSs, as shown by Figure 1. This

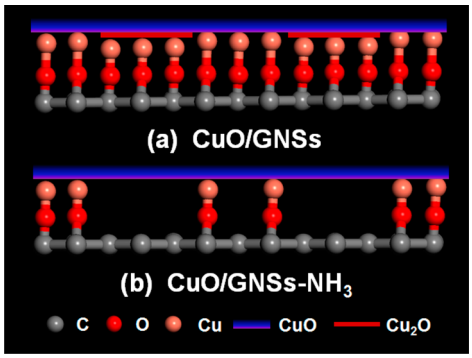

Figure 1. Schematic Diagram of (a) complex interface composed of CuO/GNSs and Cu_2O/GNSs, and (b) CuO/GNSs interface after removal of Cu_2O by $NH_3{\cdot}H_2O$.

is a perfect platform to investigate adjustment of the interface and corresponding changes in electronic structure and electrochemical performance, because we can selectively remove the Cu_2O between CuO and graphene using $NH_3{\cdot}H_2O$ and retain the interface between CuO and GNSs. By designing this interesting experiment, it can be found that the small interfacial alteration results in the obvious changes in specific capacity, cyclic performance, and diffusion dynamics of Li-ion, which just like the "butterfly effect". The results obtained may be significant for better design of metal oxide/graphene anode materials.

2. EXPERIMENTAL SECTION

2.1. Synthesis of CuO/GNSs and CuO/GNSs-NH_3. The graphene oxide used was fabricated by a modified Hummers method using natural graphite.[16]

The CuO nanosheets/GNSs composite was synthesized using the following procedure: First, $CuSO_4$ (100 mL, 0.1 M) was added to round flask in 250 mL in 20 °C with vigorous stirring. Then, the graphene oxide (37.5 mL, 3.2 mg/mL) was added to the solution; soon afterward, NaOH (7.5 mL, 4 M) was added to the mixed solution dropwise with vigorous stirring. After 30 min, the temperature was raised to 60 °C and the system continued to react for 60 min. Then, the sample was filtered and washed with deionized water. Lastly, after drying, pestling, and annealing at 300 °C for 3 h in argon gas atmosphere, the CuO/GNSs was obtained. After soaking in $NH_3{\cdot}H_2O$ for 10 min, CuO/GNSs-NH_3 was obtained.

2.2. Characterization. The obtained samples were investigated by scanning electron microscopy (SEM, ZEISS SUPRATM 55 field emission microscope), transmission electron microscopy (TEM, JEOL JEM-2100), and X-ray diffraction (XRD, Rigaku D/max-2500B2+/PCX) using Cu Kα radiation (λ = 1.5406 Å) over the range 5−90° (2θ) at room temperature.

X-ray photoelectron spectra (XPS) were recorded on a Thermo Electron Corporation ESCALAB 250 XPS spectrometer using a monochromatized Al Kα radiation (1486.6 eV) with 30 eV pass energy in 0.5 eV step over an area of 650 μm × 650 μm to the sample. All binding energies were referenced to the C 1s peak at 285 eV. Before XPS measurement, the sample was degassed under a high-vacuum condition ($<10^{-7}$ Pa) to remove the adsorbed water and oxygen. The functional group information on samples was obtained by Fourier transform infrared (FTIR, Nicolet Nexus 670). Thermogravimetry (TG) measurements were conducted on a NETZSCH STA449C simultaneous thermal instrument. The samples were heated from room temperature to 1000 °C at 5 °C/min under O_2 atmosphere. Copper elemental analysis was conducted by inductively coupled plasma (ICP) emission spectroscopy on a Shimadzu ICPS-7500 instrument.

Near-edge X-ray absorption fine structure (NEXAFS) measurements were performed at the Berliner Elektronenespeicherring für Synchrotronstrahlung (BESSY) using radiation from the Russian−German beamline. NEXAFS spectra near the C K-, O K-, and Cu L-edges were recorded in total-electron-yield (TEY) mode by monitoring the sample drain current. The spectra were normalized to the primary photon current from a gold-covered grid recorded simultaneously. The monochromatization of the incident radiation in the carbon, oxygen, and copper absorption region was ca. 80, 460, and 860 meV, respectively.

2.3. Electrochemical Measurements. Electrochemical measurements were carried out by using 2032 coin-type cells. The working electrodes were prepared by mixing the active materials, acetylene black, and poly(vinylidene difluoride) (PVDF) at a weight ratio of 8:1:1 and pasting the mixture onto foam nickel. A pure lithium sheet was used as the counter electrode. The electrolyte consisted of a solution of 1 M $LiPF_6$ in ethylene carbonate (EC)−dimethyl carbonate (DMC) (1:1 by volume). The cells were assembled in an argon-filled glovebox with the concentrations of moisture and oxygen below 1 ppm. The electrochemical performance was tested at various rates in the voltage range 0.01−3.00 V. The electrochemical impedance spectral (EIS) measurements were carried out on a ZAHNER ENNIUM electrochemical working station. For the EIS measurements, the frequency range was from 100 kHz to 10 mHz.

3. RESULTS AND DISCUSSION

3.1. Morphology and Structure of As-Prepared CuO/GNSs. TEM (Figure 2a, b) images exhibit a "sheet-on-sheet"

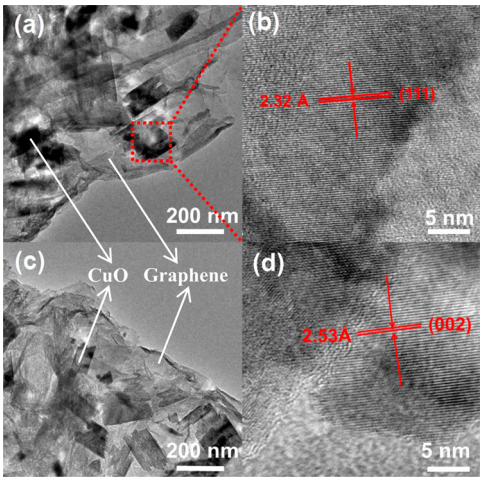

Figure 2. HRTEM images ofCuO/GNSs (a, b) and CuO/GNSs-NH_3 (c, d).

structure of CuO/GNSs composite where CuO nanosheets are anchored on the surface of graphene nanosheets. The CuO sheet has the two-dimensional width of about 200 nm and thickness of ca. 10 nm, which is similar to CuO/GNSs before annealing (Supporting Information Figure S1). The SEM and HRTEM images show the high quality of graphene after CuO removal from CuO/GNSs (Supporting Information Figure S2). Furthermore, HRTEM image displays high crystallinity of as-prepared CuO sheets. As shown by Figure 2b, it can be seen clearly the crystalline lattice of a CuO sheet, which is ca. 0.232 nm and corresponds to the (111) lattice plane of CuO.

Sharp diffraction peaks of XRD pattern (Figure 3) also indicate high crystalline structure of CuO sheets (JCPDS 48-

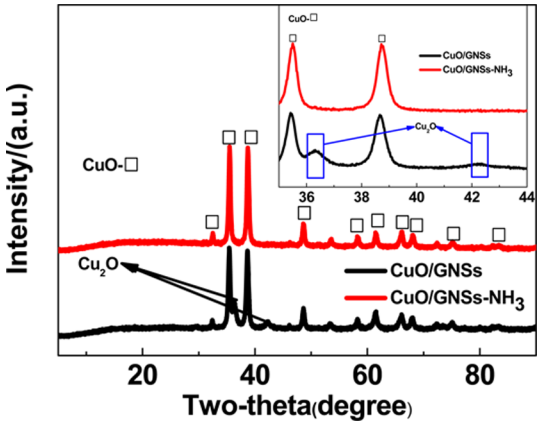

Figure 3. XRD patterns of CuO/GNSs and CuO/GNSs-NH_3.

1548). The main diffraction peaks of CuO/GNSs belong to CuO. No (002) diffraction peak of GNSs present in the XRD pattern, suggesting that CuO sheets act as a spacer to hinder the face-to-face aggregation of GNSs. It is important to note that two weak peaks, appearing at 36.4 and 42.3°, respectively, correspond to Cu_2O(JCPDS 05-0667), indicating the presence of trace amounts of Cu_2O in the sample. The formation of Cu_2O should be attributed to the reduction of small quantity of CuO by carbon during the annealing process (Supporting Information Figure S3). Therefore, it can be deduced that Cu_2O should be located between CuO and graphene, which can also be confirmed by subsequent XPS measurement. Thus, it provides a good opportunity to adjust the interface of composites using the $NH_3{\cdot}H_2O$, because Cu_2O can be dissolved in $NH_3{\cdot}H_2O$ while CuO cannot.

3.2. Morphology and Structure of CuO/GNSs-NH_3. After soaking in $NH_3{\cdot}H_2O$ for 10 min, Cu_2O diffraction peaks disappear completely in the obtained CuO/GNSs-NH_3, indicating that Cu_2O was removed. However, the intensity of diffraction peaks of CuO in the CuO/GNSs-NH_3 is almost the same as that in CuO/GNSs. Compared with those of CuO/GNSs, the morphology and the structure of CuO/GNSs-NH_3 obtained also have no obvious change, as shown by TEM images (Figure 2c, d). CuO nanosheets are still anchored tightly on GNSs and keep a high crystallinity, just as shown by Figure 2d. These results imply that only Cu_2O is removed, and CuO is not destructed by $NH_3{\cdot}H_2O$. The ICP analysis shows the concentrations of copper in CuO/GNSs and CuO/GNSs-NH_3 were 61% and 56%, respectively. Content of Cu_2O in the initial composite was ca. 4 wt % calculated by TG and ICP measurement (Supporting Information Figures S4). Although this quantity is very low, elimination of Cu_2O can affect largely the interfacial nature as well as the electrochemical performance of CuO/GNSs composites.

3.3. Change of Interfacial Bonding After Cu_2O Removal. XPS is a very effective test method to identify the nature of interfacial interaction between metal oxide and GNSs, as shown by our and others' reports.[7,9,12] Figure 4a shows that the CuO/GNSs and CuO/GNSs-NH_3 are all composed of C (285 eV, C 1s), O (532 eV, O 1s), and Cu (934 eV, Cu 2p; 77 eV, Cu 3p) elements.

The curve fitting of Cu 2p, C 1s, and O 1s was carried out by using Gaussian−Lorentzian peak shape after a Shirley background correction. In Figure 4b, the Cu $2p_{3/2}$ peak for CuO/GNSs is composed of two components at 932.5 and 933.7 eV, corresponding to Cu_2O and CuO, respectively.[17−19] After soaking in $NH_3{\cdot}H_2O$, the Cu $2p_{3/2}$ peak for CuO/GNSs-NH_3 is presented by a single component corresponding to CuO.[18] Therefore, the XPS measurement also confirms the presence of Cu_2O in the CuO/GNSs and its disappearance after the sample soaking in $NH_3{\cdot}H_2O$, which is in accord with the XRD analysis (Figure 3).

C 1s spectra of graphene (Figure 4c) in CuO/GNSs and CuO/GNSs-NH_3 can be fitted to the mainly nonoxygenated C (C═C/C—C) in aromatic rings (285 eV), and the C in C—O—C (286.1 eV) and O—C═O (289.0 eV) bonding.[7,20,21] Noticeably, intensity of the C−O−C component in residual GNSs is less by ca. 7% than that in the CuO/GNSs spectrum (Supporting Information Figure S5, Table S1), indicative of existent of bondingconnection between GNSs and copper oxide, which may be attributed to the Cu−O−C bonds.[7,9]

Subsequently, the O 1s spectra are investigated in detail, which is particularly important to confirm or disprove the existence of Cu−O−C bonds. The spectra of CuO/GNSs and CuO/GNSs-NH_3 can be fitted by three components at ca. 533.3, 531.7, and 530.1 eV, respectively. The peak at 533.3 eV should be attributed to the original oxygen in graphene oxide,[22] while the component at 530.1 eV could arise from both CuO and Cu_2O.[18,19] Here, we want to stress that it is difficult to differentiate between the peaks from CuO and Cu_2O, because, on one side, binding energies of CuO (529.6 eV) and Cu_2O

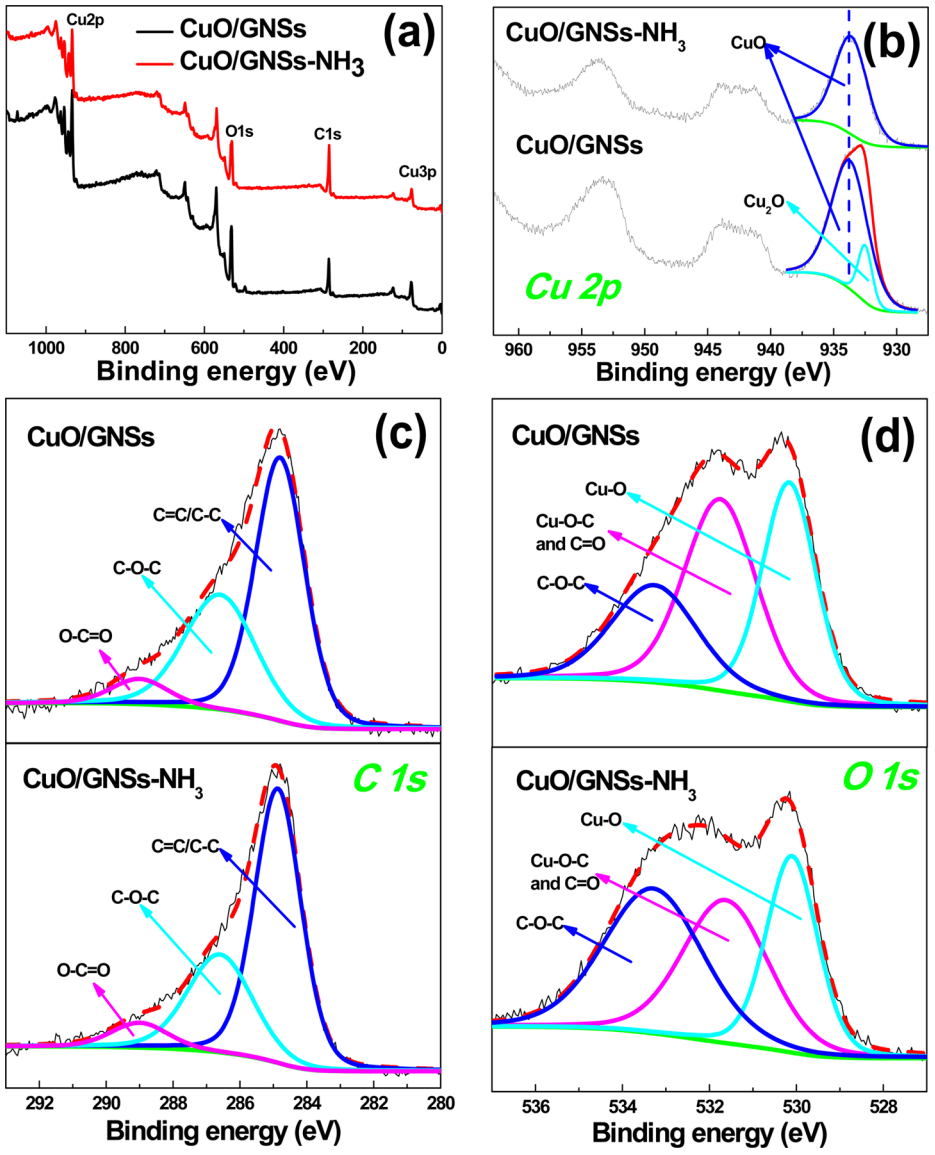

Figure 4. (a) XPS spectra of CuO/GNSs and CuO/GNSs-NH_3 and their (b) Cu 2p, (c) C 1s, and (d) O 1s spectra.

(530.3 eV) are very close to each other,[18,19] on the other hand, content of Cu_2O in the composite is only 4 wt % (Supporting Information Figure S4). The middle component at 531.7 eV should be caused by both the Cu—O—C bonding and the C═O groups in GNSs, because intensity of this peak decreases largely in the residual GNSs after removing fully CuO in the CuO/GNSs (Supporting Information Figure S5d). In addition, the Cu—O—C component can shift positively by ca. 1−3 eV than that in metal oxide according to previous reports, which is in the range 531−533 eV.[23−27] However, based on ratio of O content in C═O and C—O in the residual GNSs, we can calculate the O content from C═O in CuO/GNSs and CuO/GNSs-NH_3, respectively (detailed calculation can be seen in Supporting Information, Figure S5 and Table S2). After deducting the O content from C═O, the contents of Cu—O—C species in CuO/GNSs and CuO/GNSs-NH_3 are ca. 35% and 24%, respectively, implying a 11% decrease of Cu—O—C bonds after the $NH_3{\cdot}H_2O$ treatment (Supporting Information Figure S5 and Table S2). This result indicates that 31% of the Cu—O—C bonds between copper oxide and GNSs should be credited to Cu_2O. Therefore, it can confirm that Cu_2O should be located between CuO and graphene and be formed by reduction of partial CuO by GNSs.

Fourier transform infrared (FTIR) spectroscopy measurement also shows the changes of interfacial bonding after removal of Cu_2O. The FTIR spectra of the CuO/GNSs, CuO/GNSs-NH_3, and the remaining GNSs after removal of CuO are compared in Figure 5. The peak located at about 3430 and 1558 cm^{-1} is related to the O—H vibration and skeletal vibration of graphene, respectively.[28−30] In the FTIR spectra of CuO/GNSs and CuO/GNSs-NH_3, the peaks around 608, 497, and 414 cm^{-1} are attributed to Cu—O.[31,32] Compared with those of CuO/GNSs and CuO/GNSs-NH_3, the peaks disappear in residual GNSs. The peak presented at 1210 cm^{-1} should be attributed to the C—O—C vibration, while the peak at 1730 cm^{-1} should be caused by C═O group.[28,30] In comparison with CuO/GNSs, the peak of CuO/GNSs-NH_3 in 1081 cm^{-1} is weakened and even disappears, which is related to the C—O stretching.[29,30,33−35] It indicates that the CuO may connect with graphene in the position of C—O. In addition, the peak at 796 cm^{-1} also receded or disappeared in CuO/GNSs-NH_3 compared with the CuO/GNSs. The peak may be

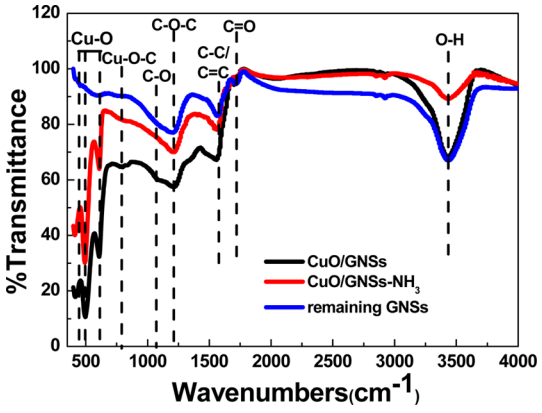

Figure 5. FTIR spectra of CuO/GNSs, CuO/GNSs-NH_3, and remaining GNSs after removal of CuO from CuO/GNSs.

related to the interactions between CuO and oxygen groups of graphene oxide, corresponding to the formation of Cu—O—C.[36]

3.4. Electronic Structure of CuO/GNSs Composites. Near edge X-ray absorption fine structure (NEXAFS) is a powerful tool for a deep understanding of electronic structure of materials. Figure 6 compares the NEXAFS spectra measured near the C K-, O K-, and Cu L-edge of CuO/GNSs and CuO/GNSs-NH_3. The features of Cu L-edge are very sensitive to the oxidation state of copper. The Cu L-edge spectrum of CuO/GNSs has two peaks at 931.3 and 933.8 eV (Figure 6a), which are ascribed to CuO and Cu_2O, respectively, according to previous reports.[37] Noticeably, the peak at 933.8 eV in the spectrum of CuO/GNSs-NH_3 disappeared completely, and only the peak at 931.3 eV remained, indicating that Cu_2O was removed fully. The O K-edge spectra confirm this conclusion. In the spectrum of CuO/GNSs, there are three peaks at 530.2, 532.5, and 534 eV (Figure 6b). The peak at 530.2 eV can be assigned to CuO, the peak at 534 eV originates from the oxygenated groups in graphene, and the peak at 532.5 eV should be attributed to Cu_2O.[37] Actually, this peak disappears from the spectrum of CuO/GNSs-NH_3. Both Cu L- and O K-edges spectra are consistent with the results of the XRD (Figure 3) and XPS (Figure 4b).

Most importantly, NEXAFS spectra analysis shows that removal of Cu_2O alters the electronic structures of graphene dramatically. Figure 6c compares the C K-edge spectra of CuO/GNSs and CuO/GNSs-NH_3. The spectrum of the former composite shows five peaks labeled A–E, respectively. The sharp peak at 285.4 eV (labeled A) is assigned to the graphitic 1s → π^* transitions, while the intense peak at 291.9 eV (labeled E) is associated with the 1s → σ^* transitions.[38−46] The weak peaks B–D located between the peak A and E should be related with the oxygen-containing functional groups and defects on graphene sheets as well as interfacial interaction between CuO/Cu_2O and graphene, according to previous reports.[42,43,45−48] After the removal of Cu_2O, the peak D at 290.4 eV is absent almost in the C K-edge spectrum of CuO/GNSs-NH_3, indicating the strong bonding between Cu_2O and GNSs. Interestingly, there is an obvious increase of the π^* resonance for CuO/GNSs-NH_3 with the disappearing of interaction between Cu_2O and GNSs, indicating the restoration of π-electron network of graphene disturbed by the Cu_2O.

Besides the changes in electronic structure and interfacial bonding, removal of Cu_2O results in the formation of micropores between CuO and GNSs. Supporting Information Figure S6 shows nitrogen adsorption−desorption isotherms and pore-size distribution curves of CuO/GNSs and CuO/GNSs-NH_3. Obviously, after soaking in $NH_3{\cdot}H_2O$ for 10 min, the new micropores in CuO/GNSs-NH_3 are presented at ca. 1.36 and 1.48 nm, which never appeared in the CuO/GNSs. Simultaneously, the specific surface area of CuO/GNSs-NH_3 increased to 55 m^2/g from 50 m^2/g of CuO/GNSs. The increase of specific surface area and presence of new micropores will create new position for Li-ion storage in CuO/GNSs-NH_3.

3.5. Influence of Change of Interfacial Nature on Electrochemical Performance. To confirm the influence of the change in interfacial interaction in composite on the electrochemical performance, specific capacity, cyclic performance, as well as dynamic parameters of CuO/GNSs and CuO/GNSs-NH_3 as anode materials for lithium-ion batteries were

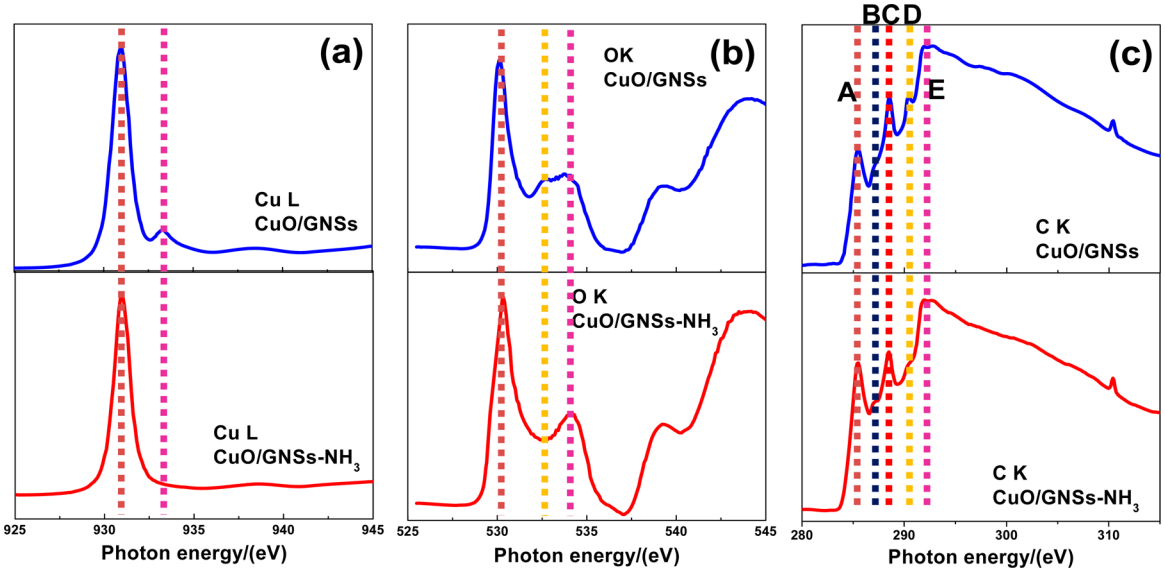

Figure 6. NEXAFS spectra near (a) Cu L-, (b) O K-, and (c) C K-edge of CuO/GNSs and CuO/GNSs-NH_3.

dx.doi.org/10.1021/am505186a | ACS Appl. Mater. Interfaces 2014, 6, 17236−17244

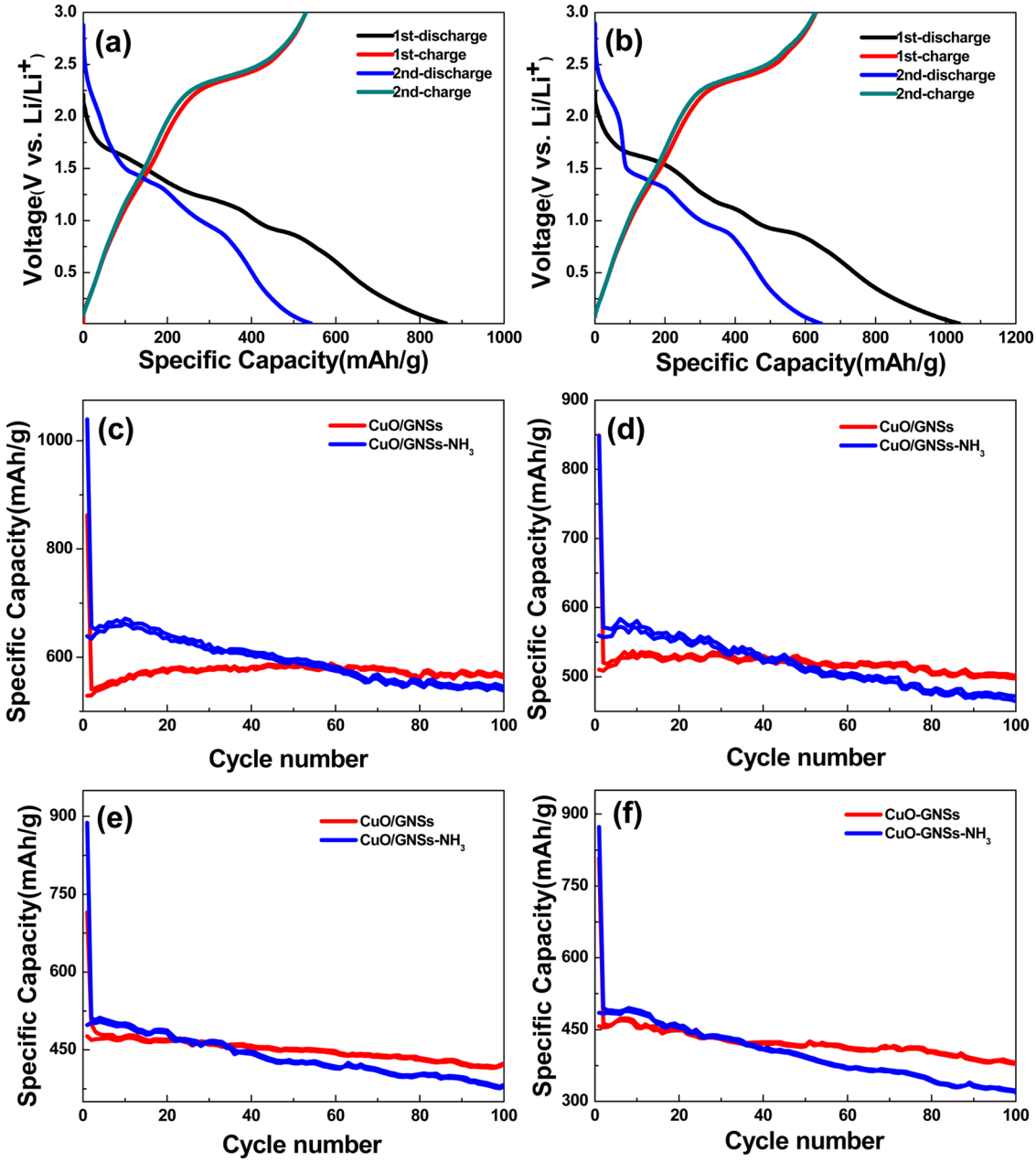

Figure 7. Charge−discharge curves of CuO/GNSs (a) and CuO/GNSs-NH_3 (b). The cycle performance of CuO/GNSs and CuO/GNSs-NH_3 at a current density of 100 (c), 200 (d), 500 (e), and 800 mAg^{-1} (f).

evaluated by galvanostatic charge/discharge measurement. It was found that the discharge/charge voltage profiles were similar, implying that CuO is the key specific capacity contributor of CuO/GNSs and CuO/GNSs-NH_3 (Figure 7a, b). CuO/GNSs and CuO/GNSs-NH_3 all have three pseudoplateaus (2.5−2.0, 1.5−1.25, and 1.0 V vs Li^+/Li, respectively) for the reaction of Li and CuO, corresponding to the multistep electrochemical Li reaction process.[8,49] We also found CuO/GNSs and CuO/GNSs-NH_3 have a discharge slope between 0.5 and 0.01 V, which is corresponding to the reaction of Li-ion and graphene.[8]

A change of interface leads to increase of specific capacity of CuO/GNSs-NH_3. From Figure 7c, the first discharge specific capacity (Li-insertion) and reversible capacity of CuO/GNSs are 862 and 529 $mAhg^{-1}$ at a current density of 100 mAg^{-1}, respectively. After removing Cu_2O, the first discharge capacity and reversible capacity of CuO/GNSs-NH_3 electrode increases to 1039 and 639 $mAhg^{-1}$, respectively. Noticeably, reversible capacity improves by ca. 21% after adjusting the interface. However, there is a little difference in the theoretical specific capacities of CuO/GNSs and CuO/GNSs-NH_3, which are ca. 592 and 589 $mAhg^{-1}$ calculated from the theoretic capacity of CuO (674 $mAhg^{-1}$), Cu_2O (375 $mAhg^{-1}$), and the reversible capacity of GNSs (308 $mAhg^{-1}$, Supporting Information Figure S8). Therefore, it should be attributed to the change of specific surface area as well as presence of micropores due to the fact that micropores own the ability of Li-ion storage, as shown by previous reports.[50−53]

However, weakening of interfacial interaction would produce an unfavorable effect on cyclic performance. During the initial 18 cycles, no any fade of specific capacity occurs to CuO/GNSs-NH_3 at 100 $mAhg^{-1}$ (Figure 7c). Thereafter, its capacity

begins to decrease gradually. After 100 cycles, the discharge specific capacity of the CuO/GNSs-NH_3 is 538 $mAhg^{-1}$, which is ca. 84% of the first reversible capacity. Compared with CuO/GNSs-NH_3, CuO/GNSs exhibit better cyclic performance. After 100 cycles, the result shows that its capacity not only has no any decrease but, on the contrary, increases to 563 $mAhg^{-1}$, which is even higher than that of CuO/GNSs-NH_3. This indicates that CuO/GNSs-NH_3 with weaker interfacial interaction is hard to resist the repeating insertion/desertion of Li-ion.

Weakening of interfacial interaction would also be unhelpful to the improvement of rate-performance (Supporting Information Table S3). When the current density increases to 200 mAg^{-1}, the difference of the first reversible capacity between CuO/GNSs (510 $mAhg^{-1}$) and CuO/GNSs-NH_3 (560 $mAhg^{-1}$) shrinks to 50 $mAhg^{-1}$. The difference of their first reversible capacities shrinks in further to 22 $mAhg^{-1}$ at 500 mAg^{-1}. Gradual decrease of the difference with the increase of current density indicates poorer rate-performance of CuO/GNSs-NH_3. Meanwhile, cyclic stability of CuO/GNSs-NH_3 gets worse and worse compared to that of CuO/GNSs with the increase of current density. At 100 mAg^{-1}, the discharge specific capacity of the CuO/GNSs after 100 cycles can retain 107% of its first reversible capacity while retention rate of capacity of CuO/GNSs-NH_3 can only be 84%. When the current density increases to 800 mAg^{-1}, retention rate of capacity of CuO/GNSs is still up to 83%. In contrast, retention rate of CuO/GNSs-NH_3 only keeps at ca. 66%.

To reveal the reasons for changes of electrochemical performance after adjusting interfacial interaction, the kinetics of both CuO/GNSs and CuO/GNSs-NH_3 electrodes were investigated by the electrochemical impedance spectroscopy measurement (Supporting Information Figure S7). It can be seen that the film resistance (R_f) and charge-transfer resistance (R_{ct}) of CuO/GNSs are ca. 13.5 and 58.0 Ω, respectively. Both the R_f (49.8 Ω) and R_{ct} (152.3 Ω) of CuO/GNSs-NH_3 are much larger than those of the CuO/GNSs electrode, which leads to poorer rate-performance of CuO/GNSs-NH_3. Generally, improvement of electrochemical performance of graphene-based metal oxide anode materials is attributed to formation of a better conductive network of GNSs. The transfer of electron in graphene-based metal oxide composites should be affected by the resistance in the graphene basal plane (R_g) as well as that between metal oxide and graphene sheets ($R_{MO\text{-}g}$). R_g of CuO/GNSs-NH_3 should be lower than that of CuO/GNSs due to the restoration of π network of graphene after removing Cu_2O as shown by NEXAFS measurements. However, the overall charger-transfer resistance of CuO/GNSs-NH_3 is nearly 3 times higher than that of CuO/GNSs, so R_{MO}-g of CuO/GNSs-NH_3 should be much higher than that of CuO/GNSs. It indicates that the covalent interaction of Cu−O−C bonds between CuO and GNSs plays an important role for electron transfer.

Due to undergoing the conversion reaction during the discharge/charge process, a recent report indicated that reconstruction of MnO nanosheet on graphene into ultrathin nanoparticles could occur during the cycling, which will be helpful to keep superior electrochemical performance of MnO/graphene.[54] Therefore, it is also very interesting to observe the effect of interfacial nature on the morphology conversion of CuO nanosheet on graphene. To observe the change of morphology of CuO/GNSs and CuO/GNSs-NH_3, we have opened the battery and observed the composite after the discharge/charge cycles by TEM. Supporting Information Figure S9 shows the CuO nanosheets on graphene for both CuO/GNSs and CuO/GNSs-NH_3 have changed into small nanoparticles, which is very consistent with that in MnO/graphene composite.[54] However, the average size of CuO/GNSs (ca. 3.5 nm) after cycle was obviously much smaller than that of CuO/GNSs-NH_3 (ca. 7 nm), and the distribution of CuO/GNSs was more uniform than that of CuO/GNSs-NH_3, which should be attributed to the stronger interfacial interaction in CuO/GNSs than that in CuO/GNSs-NH_3. The smaller particles of CuO/GNSs will lead stronger interaction between CuO and graphene due to the more contact points, which will benefit to limiting the aggregation of active materials upon cycling.[7,54] Meanwhile, another report also shows that smaller particles formed from conversion reaction is more helpful to reversibility of electrode material.[55] Therefore, the CuO/GNSs electrode showed better cyclic and rate performance.

4. CONCLUSIONS AND OUTLOOK

In summary, CuO nanosheets/GNSs composites with a little Cu_2O were utilized as a model to illustrate directly the interfacial adjustment as well as its deep influence on the Li-ion storage performance. It can be found that Cu−O−C bonds were formed on interfaces both between CuO and GNSs and between Cu_2O and GNSs. The small interfacial alteration by removal of Cu_2O led to the obvious changes in electronic structure and electrochemical performance of composite anode materials, including the large increase of reversible capacity, degradation of cyclic stability and rate-performance, and obvious increase of charge-transfer resistance. Therefore, a small adjustment of interfacial interaction can trigger a "butterfly effect" in the Li-ion storage of graphene-based composite anodes, which should be a new pathway to design advanced graphene-based composites in the other application fields such as sensors, catalysis, fuel cells, and solar cells.

■ ASSOCIATED CONTENT

Supporting Information

SEM and HRTEM images of CuO/GNSs before annealing and after removing CuO, XRD pattern of CuO/GNSs before annealing, TG curve, nitrogen adsorption−desorption isotherm, pore-size distribution, AC impedance spectra and specific capacity value of CuO/GNSs and CuO/GNSs-NH_3, XPS spectra of CuO/GNSs after removal of CuO, the electrochemical performance of remaining GNSs after removal of CuO from CuO/GNSs. HRTEM images of CuO/GNSs and CuO/GNSs-NH3 after the charge-discharge reaction. This material is available free of charge via the Internet at http://pubs.acs.org.

■ AUTHOR INFORMATION

Corresponding Author

*Email: songhh@mail.buct.edu.cn.

Author Contributions

‖X.Zhang and J.Zhou contributed equally.

Notes

The authors declare no competing financial interest.

■ ACKNOWLEDGMENTS

This work was supported by the National Natural Science Foundation of China (51202009 and 51272019), New

Teachers' Fund for Doctor Stations, Ministry of Education of China (20120010120004), Foundation of Excellent Doctoral Dissertation of Beijing City (YB20121001001), the Russian foundation for Basic Research (grants 13-03-90920 and 14-03-91057), and the bilateral Program "Russian-German Laboratory at BESSY".

REFERENCES

(1) Poizot, P.; Laruelle, S.; Grugeon, S.; Dupont, L.; Tarascon, J. Nano-Sized Transition-Metal Oxides as Negative-Electrode Materials for Lithium-Ion Batteries. *Nature* **2000**, *407*, 496−499.
(2) Huang, X. H.; Tu, J. P.; Zhang, B.; Zhang, C. Q.; Li, Y.; Yuan, Y. F.; Wu, H. M. Electrochemical Properties of NiO−Ni Nanocomposite as Anode Material for Lithium Ion Batteries. *J. Power Sources* **2006**, *161*, 541−544.
(3) Zhang, P.; Guo, Z. P.; Liu, H. K. Submicron-Sized Cube-Like Alpha-Fe_2O_3Agglomerates as an Anode Material for Li-Ion Batteries. *Electrochim. Acta* **2010**, *55*, 8521−8526.
(4) Ke, F.-S.; Huang, L.; Wei, G.-Z.; Xue, L.-J.; Li, J.-T.; Zhang, B.; Chen, S.-R.; Fan, X.-Y.; Sun, S.-G. One-Step Fabrication of CuO Nanoribbons Array Electrode and Its Excellent Lithium Storage Performance. *Electrochim. Acta* **2009**, *54*, 5825−5829.
(5) Lu, Y.; Wang, Y.; Zou, Y.; Jiao, Z.; Zhao, B.; He, Y.; Wu, M. Macroporous Co_3O_4 Platelets with Excellent Rate Capability as Anodes for Lithium Ion Batteries. *Electrochem. Commun.* **2010**, *12*, 101−105.
(6) Wang, H.; Dai, H. Strongly Coupled Inorganic−Nano-Carbon Hybrid Materials for Energy Storage. *Chem. Soc. Rev.* **2013**, *42*, 3088−3113.
(7) Zhou, J.; Song, H.; Ma, L.; Chen, X. Magnetite/Graphene Nanosheet Composites: Interfacial Interaction and Its Impact on the Durable High-Rate Performance in Lithium-Ion Batteries. *RSC Adv.* **2011**, *1*, 782−791.
(8) Zhou, J.; Ma, L.; Song, H.; Wu, B.; Chen, X. Durable High-Rate Performance of CuO Hollow Nanoparticles/Graphene-Nanosheet Composite Anode Material for Lithium-Ion Batteries. *Electrochem. Commun.* **2011**, *13*, 1357−1360.
(9) Zhou, G.; Wang, D.-W.; Yin, L.-C.; Li, N.; Li, F.; Cheng, H.-M. Oxygen Bridges between NiO Nanosheets and Graphene for Improvement of Lithium Storage. *ACS Nano* **2012**, *6*, 3214−3223.
(10) Wang, H.; Robinson, J. T.; Diankov, G.; Dai, H. Nanocrystal Growth on Graphene with Various Degrees of Oxidation. *J. Am. Chem. Soc.* **2010**, *132*, 3270−3271.
(11) Liang, Y.; Li, Y.; Wang, H.; Dai, H. Strongly Coupled Inorganic/Nanocarbon Hybrid Materials for Advanced Electrocatalysis. *J. Am. Chem. Soc.* **2013**, *135*, 2013−36.
(12) Liang, Y.; Li, Y.; Wang, H.; Zhou, J.; Wang, J.; Regier, T.; Dai, H. Co_3O_4Nanocrystals on Graphene as a Synergistic Catalyst for Oxygen Reduction Reaction. *Nat. Mater.* **2011**, *10*, 780−786.
(13) Wu, Z.-S.; Ren, W.; Wen, L.; Gao, L.; Zhao, J.; Chen, Z.; Zhou, G.; Li, F.; Cheng, H.-M. Graphene Anchored with Co_3O_4 Nanoparticles as Anode of Lithium Ion Batteries with Enhanced Reversible Capacity and Cyclic Performance. *ACS Nano* **2010**, *4*, 3187−3194.
(14) Zhou, G.; Wang, D.-W.; Li, F.; Zhang, L.; Li, N.; Wu, Z.-S.; Wen, L.; Lu, G. Q.; Cheng, H.-M. Graphene-Wrapped Fe_3O_4Anode Material with Improved Reversible Capacity and Cyclic Stability for Lithium Ion Batteries. *Chem. Mater.* **2010**, *22*, 5306−5313.
(15) Wang, H.; Cui, L.-F.; Yang, Y.; Sanchez Casalongue, H.; Robinson, J. T.; Liang, Y.; Cui, Y.; Dai, H. Mn_3O_4−Graphene Hybrid as a High-Capacity Anode Material for Lithium Ion Batteries. *J. Am. Chem. Soc.* **2010**, *132*, 13978−13980.
(16) Hummers, W. S., Jr; Offeman, R. E. Preparation of Graphitic Oxide. *J. Am. Chem. Soc.* **1958**, *80*, 1339−1339.
(17) Espinos, J.; Morales, J.; Barranco, A.; Caballero, A.; Holgado, J.; Gonzalez-Elipe, A. Interface Effects for Cu, CuO, and Cu_2O Deposited on SiO_2 and ZrO_2. XPS Determination of the Valence State of Copper in Cu/SiO_2 and Cu/ZrO_2Catalysts. *J. Phys. Chem. B* **2002**, *106*, 6921−6929.
(18) Poulston, S.; Parlett, P.; Stone, P.; Bowker, M. Surface Oxidation and Reduction of CuO and Cu_2O Studied Using XPS and XAES. *Surf. Interface Anal.* **1996**, *24*, 811−820.
(19) Ghijsen, J.; Tjeng, L.; Van Elp, J.; Eskes, H.; Westerink, J.; Sawatzky, G.; Czyzyk, M. Electronic Structure of Cu_2O and CuO. *Phys. Rev. B* **1988**, *38*, 11322.
(20) Qi, Y.; Eskelsen, J. R.; Mazur, U.; Hipps, K. W. Fabrication of Graphene with CuO Islands by Chemical Vapor Deposition. *Langmuir* **2012**, *28*, 3489−3493.
(21) Hsu, Y.-W.; Hsu, T.-K.; Sun, C.-L.; Nien, Y.-T.; Pu, N.-W.; Ger, M.-D. Synthesis of CuO/Graphene Nanocomposites for Non-enzymatic Electrochemical Glucose Biosensor Applications. *Electrochim. Acta* **2012**, *82*, 152−157.
(22) Yang, D.; Velamakanni, A.; Bozoklu, G.; Park, S.; Stoller, M.; Piner, R. D.; Stankovich, S.; Jung, I.; Field, D. A.; Ventrice, C. A., Jr Chemical Analysis of Graphene Oxide Films after Heat and Chemical Treatments by X-ray Photoelectron and Micro-Raman Spectroscopy. *Carbon* **2009**, *47*, 145−152.
(23) Kataby, G.; Cojocaru, M.; Prozorov, R.; Gedanken, A. Coating Carboxylic Acids on Amorphous Iron Nanoparticles. *Langmuir* **1999**, *15*, 1703−1708.
(24) Dicke, C.; Morstein, M.; Hähner, G. Surface Inorganic Chemistry: The Reaction of Hydroxyl-Terminated Thiols on Gold with a Zirconium Coordination Compound. *Langmuir* **2002**, *18*, 336−344.
(25) Serghini-Monim, S.; Norton, P.; Puddephatt, R.; Pollard, K.; Rasmussen, J. Adsorption of a Silver Chemical Vapor Deposition Precursor on Polyurethane and Reduction of the Adsorbate to Silver Using Formaldehyde. *J. Phys. Chem. B* **1998**, *102*, 1450−1458.
(26) Combellas, C.; Delamar, M.; Kanoufi, F.; Pinson, J.; Podvorica, F. I. Spontaneous Grafting of Iron Surfaces by Reduction of Aryldiazonium Salts in Acidic or Neutral Aqueous Solution. Application to the Protection of Iron Against Corrosion. *Chem. Mater.* **2005**, *17*, 3968−3975.
(27) Hurley, B. L.; McCreery, R. L. Covalent Bonding of Organic Molecules to Cu and Al Alloy 2024 T3 Surfaces via Diazonium Ion Reduction. *J. Electrochem. Soc.* **2004**, *151*, B252−B259.
(28) Srivastava, R. K.; Srivastava, S.; Narayanan, T. N.; Mahlotra, B. D.; Vajtai, R.; Ajayan, P. M.; Srivastava, A. Functionalized Multilayered Graphene Platform for Urea Sensor. *ACS Nano* **2012**, *6*, 168−175.
(29) Xiao, L.; Liao, L.; Liu, L. Chemical Modification of Graphene Oxide with Carbethoxycarbene under Microwave Irradiation. *Chem. Phys. Lett.* **2013**, *556*, 376−379.
(30) Zhao, Y.; Song, X.; Song, Q.; Yin, Z. A Facile Route to the Synthesis Copper Oxide/Reduced Graphene Oxide Nanocomposites and Electrochemical Detection of Catechol Organic Pollutant. *CrystEngComm* **2012**, *14*, 6710−6719.
(31) Zou, G.; Li, H.; Zhang, D.; Xiong, K.; Dong, C.; Qian, Y. Well-Aligned Arrays of CuO Nanoplatelets. *J. Phys. Chem. B* **2006**, *110*, 1632−1637.
(32) Yu, Q.; Huang, H.; Chen, R.; Wang, P.; Yang, H.; Gao, M.; Peng, X.; Ye, Z. Synthesis of CuO Nanowalnuts and Nanoribbons from Aqueous Solution and Their Catalytic and Electrochemical Properties. *Nanoscale* **2012**, *4*, 2613−2620.
(33) Guo, H.-L.; Wang, X.-F.; Qian, Q.-Y.; Wang, F.-B.; Xia, X.-H. A Green Approach to the Synthesis of Graphene Nanosheets. *ACS Nano* **2009**, *3*, 2653−2659.
(34) Xu, J.; Wang, K.; Zu, S.-Z.; Han, B.-H.; Wei, Z. Hierarchical Nanocomposites of Polyaniline Nanowire Arrays on Graphene Oxide Sheets with Synergistic Effect for Energy Storage. *ACS Nano* **2010**, *4*, 5019−5026.
(35) Zhu, Z.; Ma, L.; Su, M.; Liu, D.; Wang, Z. Preparation and Application of Thionin-Bridged Graphene-Gold Nanoparticle Nanohybrids. *J. Mater. Chem. B* **2013**, *1*, 1432−1438.
(36) Mabayoje, O.; Seredych, M.; Bandosz, T. J. Enhanced Reactive Adsorption of Hydrogen Sulfide on the Composites of Graphene/Graphite Oxide with Copper (Hydr) Oxychlorides. *ACS Appl. Mater. Interfaces* **2012**, *4*, 3316−3324.

(37) Nachimuthu, P.; Thevuthasan, S.; Kim, Y. J.; Lea, A. S.; Shutthanandan, V.; Engelhard, M. H.; Baer, D. R.; Chambers, S. A.; Shuh, D. K.; Lindle, D. W.; Gullikson, E. M.; Perera, R. C. C. Investigation of Copper(I) Oxide Quantum Dots by Near-Edge X-ray Absorption Fine Structure Spectroscopy. *Chem. Mater.* **2003**, *15*, 3939−3946.
(38) Zhang, L.; Ji, L.; Glans, P.-A.; Zhang, Y.; Zhu, J.; Guo, J. Electronic Structure and Chemical Bonding of a Graphene Oxide−Sulfur Nanocomposite for Use in Superior Performance Lithium−Sulfur Cells. *Phys. Chem. Chem. Phys.* **2012**, *14*, 13670−13675.
(39) Lai, L.; Yang, H.; Wang, L.; Teh, B. K.; Zhong, J.; Chou, H.; Chen, L.; Chen, W.; Shen, Z.; Ruoff, R. S.; Lin, J. Preparation of Supercapacitor Electrodes through Selection of Graphene Surface Functionalities. *ACS Nano* **2012**, *6*, 5941−5951.
(40) Lee, V.; Whittaker, L.; Jaye, C.; Baroudi, K. M.; Fischer, D. A.; Banerjee, S. Large-Area Chemically Modified Graphene Films: Electrophoretic Deposition and Characterization by Soft X-ray Absorption Spectroscopy. *Chem. Mater.* **2009**, *21*, 3905−3916.
(41) Lee, V.; Park, C.; Jaye, C.; Fischer, D. A.; Yu, Q.; Wu, W.; Liu, Z.; Bao, J.; Pei, S.-S.; Smith, C. Substrate Hybridization and Rippling of Graphene Evidenced by Near-Edge X-ray Absorption Fine Structure Spectroscopy. *J. Phys. Chem. Lett.* **2010**, *1*, 1247−1253.
(42) Brandes, J. A.; Cody, G. D.; Rumble, D.; Haberstroh, P.; Wirick, S.; Gelinas, Y. Carbon K-Edge XANES Spectromicroscopy of Natural Graphite. *Carbon* **2008**, *46*, 1424−1434.
(43) Dubin, S.; Gilje, S.; Wang, K.; Tung, V. C.; Cha, K.; Hall, A. S.; Farrar, J.; Varshneya, R.; Yang, Y.; Kaner, R. B. A One-Step, Solvothermal Reduction Method for Producing Reduced Graphene Oxide Dispersions in Organic Solvents. *ACS Nano* **2010**, *4*, 3845−3852.
(44) Pacile, D.; Meyer, J. C.; Rodriguez, A. F.; Papagno, M.; Gomez-Navarro, C.; Sundaram, R. S.; Burghard, M.; Kern, K.; Carbone, C.; Kaiser, U. Electronic Properties and Atomic Structure of Graphene Oxide Membranes. *Carbon* **2011**, *49*, 966−972.
(45) Zhan, D.; Ni, Z.; Chen, W.; Sun, L.; Luo, Z.; Lai, L.; Yu, T.; Wee, A. T. S.; Shen, Z. Electronic Structure of Graphite Oxide and Thermally Reduced Graphite Oxide. *Carbon* **2011**, *49*, 1362−1366.
(46) Liang, Y.; Wang, H.; Zhou, J.; Li, Y.; Wang, J.; Regier, T.; Dai, H. Covalent Hybrid of Spinel Manganese−Cobalt Oxide and Graphene as Advanced Oxygen Reduction Electrocatalysts. *J. Am. Chem. Soc.* **2012**, *134*, 3517−3523.
(47) Zhang, L.; Pollak, E.; Wang, W.-C.; Jiang, P.; Glans, P.-A.; Zhang, Y.; Cabana, J.; Kostecki, R.; Chang, C.; Salmeron, M.; Zhu, J.; Guo, J. Electronic Structure Study of Ordering and Interfacial Interaction in Graphene/Cu Composites. *Carbon* **2012**, *50*, 5316−5322.
(48) Saxena, S.; Tyson, T. A.; Negusse, E. Investigation of the Local Structure of Graphene Oxide. *J. Phys. Chem. Lett.* **2010**, *1*, 3433−3437.
(49) Zheng, S.-F.; Hu, J.-S.; Zhong, L.-S.; Song, W.-G.; Wan, L.-J.; Guo, Y.-G. Introducing Dual Functional CNT Networks into CuO Nanomicrospheres toward Superior Electrode Materials for Lithium-Ion Batteries. *Chem. Mater.* **2008**, *20*, 3617−3622.
(50) Dahn, J.; Zheng, T.; Liu, Y.; Xue, J. Mechanisms for Lithium Insertion in Carbonaceous Materials. *Science* **1995**, *270*, 590−593.
(51) Fukui, H.; Nakata, N.; Dokko, K.; Takemura, B.; Ohsuka, H.; Hino, T.; Kanamura, K. Lithiation and Delithiation of Silicon Oxycarbide Single Particles with a Unique Microstructure. *ACS Appl. Mater. Interfaces* **2011**, *3*, 2318−2322.
(52) Li, H.; Wang, Q.; Shi, L.; Chen, L.; Huang, X. Nanosized SnSb alloy Pinning on Hard Non-Graphitic Carbon Spherules as Anode Materials for a Li Ion Battery. *Chem. Mater.* **2002**, *14*, 103−108.
(53) Kang, D.-K.; Corno, J. A.; Gole, J. L.; Shin, H.-C. Microstructured Nanopore-Walled Porous Silicon as an Anode Material for Rechargeable Lithium Batteries. *J. Electrochem. Soc.* **2008**, *155*, A276−A281.
(54) Sun, Y.; Hu, X.; Luo, W.; Xia, F.; Huang, Y. Reconstruction of Conformal Nanoscale MnO on Graphene as a High-Capacity and Long-Life Anode Material for Lithium Ion Batteries. *Adv. Funct. Mater.* **2013**, *23*, 2436−2444.
(55) Wang, F.; Robert, R.; Chernova, N. A.; Pereira, N.; Omenya, F.; Badway, F.; Hua, X.; Ruotolo, M.; Zhang, R.; Wu, L.; Volkov, V.; Su, D.; Key, B.; Whittingharn, M. S.; Grey, C. P.; Amatucci, G. G.; Zhu, Y.; Graetz, J. Conversion Reaction Mechanisms in Lithium Ion Batteries: Study of the Binary Metal Fluoride Electrodes. *J. Am. Chem. Soc.* **2011**, *133*, 18828−18836.